





Triple Diffusive MHD Casson Fluid Flow Over a Vertical Wall with Convective Boundary Conditions

Sushma Shankar ¹ , Suresh Babu Ramakrishna ^{1,*} , Neeraja Gullapalli ¹ , Nancy Samuel ¹ 

¹ Department of Mathematics, M S Ramaiah Institute of Technology, Bangalore-560 054, Karnataka, India; sushmsrit@gmail.com (S.S.); sureshbabu_r80@yahoo.co.in (S.B.R.); gneerajamaths@gmail.com (N.G.); samuelnancy1984@gmail.com (N.S.);

* Correspondence: sureshbabu_r80@yahoo.co.in;

Scopus Author ID 57199323358

Received: 12.01.2021; Revised: 7.02.2021; Accepted: 10.02.2021; Published: 17.02.2021

Abstract: In this article, we study, effects of triple diffusive on a mixed convective viscous flow of an MHD Casson fluid through a vertical permeable wall numerically with convective BC's. The governing equations are modeled and derived for the triple diffusive boundary layer flow to examine the fluid's nature under the influence of thermal conductivity and solutal diffusivity. Using an effective and suitable similarity transformation, highly non-linear coupled PDE's are reduced to a series of coupled ODE's and are solved by the Shooting technique with the help of the integral scheme of Runge Kutta-Fehlberg. To know the fluid properties' behavior, a numerical computation has been carried out for the non-dimensional parameters, which control the flow and demonstrated through plots such as permeability, convective parameter, Casson parameter, and buoyancy ratio parameters of the physical system. In the absence of a few non-dimensional parameters, present findings are compared with previously published work to validate our numerical scheme and found to be in good agreement with up to six decimal places of accuracy.

Keywords: triple diffusive; MHD; Casson fluid; mixed convection; vertical wall; shooting technique.

© 2021 by the authors. This article is an open-access article distributed under the terms and conditions of the Creative Commons Attribution (CC BY) license (<https://creativecommons.org/licenses/by/4.0/>).

1. Introduction

The study of heat and mass transfer received considerable interest in many theoretical and experimental/practical aspects because of its various applications in industry, scientific, and engineering processes. In the literature, such problems are dealt with the Newtonian/non-Newtonian and non-Darcian fluids through/past a vertical surface with different boundary conditions. References and comprehensive literature surveys related to porous medium have been described by Nield and Bejan [1]. The advancement of modern technologies has demanded the study of fluid streams, which encompass the interaction of numerous phenomena. Double diffusion appears in buoyancy compelled flow due to the amalgamation of temperature and concentration gradients; many authors had studied such a study in a porous medium. Kumari *et al.* [2] have been studied mixed convection flow under the influence of the magnetic field with an isotropic solid matrix and dissipation. Boussinesq approximations are tested by Mamou *et al.* [3] for a double-diffusive natural convective flow of a Darcy model in an inclined porous layer. The boundary layer flow of a sloping plate with IHG and chemical reaction in a saturated porous medium by Patil *et al.* [4], and the studied under the impact of Soret effect by Murthy *et al.* [5]. Mallikarjuna *et al.* [6] examined non-uniform heat sources' effects on a rotary device over a plate fixed in a non-Darcy porous medium. The results of

double-diffusive on mixed convective viscous fluid through a plate with variable fluid properties were discussed by Suresh Babu *et al.* [7].

However, suppose there are gradients of more than two diffusing elements that exist. In that case, the species concentration and temperature are known as multiple diffusive convection. The presence of more than one chemical dissolved in a liquid mixture describes common phenomena such as transport of toxic elements, latent water flow, and acid flow. Triple diffusion comprises three constituents with different diffusivities. Application of triple diffusive convection can be noticed in the modeling of medical airing tool for the study of anomalies in fatty acid, encompassing numerous constituents such as saturated fat (Cholesterol-low-density lipoproteins, high-density lipoproteins) and triglycerides, which retain dissimilar diffusivities. However, triple diffusion in a non-Newtonian fluid has practical applications in many medical sciences and bioengineering. For example, aqueous suspensions of deoxyribonuc DNA contain more than two independently diffusing constituents with dissimilar diffusivities found in the book by Rionero *et al.* [8]. The triple diffusion in a Newtonian or non-Newtonian fluid has been studied extensively for a flat plate with convective boundary conditions by Khan *et al.* [9], stability analysis of a viscoelastic fluid by Raghunatha *et al.* [10], NaCl-water and sucrose water solutions by Patil *et al.* [11, 12], along with a stretching sheet with variable thickness by Nancy Samuel [13], for a duct by Umavathi *et al.* [14], linear stability analysis of a Maxwell fluid by Raghunatha *et al.* [15], for various porous cavities by Khan *et al.* [16], entropy generation analysis by Khan *et al.* [17] and diffusion of species using tangent hyperbolic rheology by Nawaz *et al.* [18].

Lateral inequality occurs in the direction of the deposited charge, and the magnetic fields applied between the opposite positions (perpendicular to the charge flow) induce currents of perpendicular, magnetic, and electrical currents to both magnetic fields. An electrically conducting fluid with an external constraint of the magnetic field can be regulated. The transfer rate can also be controlled. With this point of view, various industrial applications can be seen in many branches of sciences and technology like cooling nuclear reactors, boundary layer control in aerodynamics, plasma studies, petroleum industries, and crystal growth, etc. Hence, the authors are received new attention for the study of most general contexts of magnetohydrodynamics (MHD) with the external forces of an electrically conducting magnetic field. Casson fluid is a non-Newtonian fluid that exhibits stress on yield and requires high temperature for industrial and engineering problems. Isa *et al.* [19] investigated numerically MHD mixed convection flow over a stretching sheet. Sharada *et al.* [20] examined Soret, Dufour, radiation, and chemical reaction effects on MHD flow of a Casson fluid over an exponentially stretching surface. By considering convective boundary conditions, Hayat *et al.* [21] studied the stagnation point flow of a Casson fluid for stretching surface and John *et al.* [22] MHD Casson fluid over a plate with Joule heating. Srinivasa *et al.* [23] and Saqib *et al.* [26] examined numerically unsteady MHD Casson fluid flow over a vertical surface with an angle of inclination, constant heat flux, chemical reaction, whereas Muthuraj *et al.* [24] examined for stretching walls. Kataria *et al.* [25] studied heat, mass transfer characteristics of a MHD Casson fluid over an oscillating plate with ramped wall temperature. Heat transfer study of the unstable MHD Casson fluid over a plate with arbitrary wall shear and the constant temperature was analyzed by Khan *et al.* [27]. Vijaya Bhaskar *et al.* [28] investigated numerical analysis of MHD Casson fluid flow over an exponentially moving plate with a ramped wall temperature and surface concentration. Under the influence of thermal radiation and heat source/sink parameters along with the slip parameters, Sumera *et al.* [29] studied 2D heat

transfer flow of a Casson-dependent nanofluid over a vertical stretching and shrinking sheet. The non-linear thermal radiated triple diffuse flow of a Casson nanofluid along a horizontal plate was studied by Manjappa *et al.* [30] and is theoretically investigated in the presence of more than one solution diffused in mixtures of fluids. Rao *et al.* [31] studied 3D heat mass transfer MHD motion over a stretching surface with Brownian flow, thermophoresis, and Dufour effects and found that the transfer rate of energy and concentration in the Newtonian fluid is relatively low compared to the non-Newtonian fluid. Computational analysis has been done by Lund *et al.* [32] on MHD micropolar fluid on a shrinking surface under the Joule effect and viscous dissipation. Ramanna *et al.* [33] investigated triple diffusion encoding MRI to measure the intra, and extra axonal diffusion tensors.

According to the authors' knowledge and the above literature, no research has been carried out to examine the effect of triple diffusion on an MHD Casson fluid with convective boundary conditions. However, the heat and mass diffusion components are always coupled in most real-world problems. This fact motivates us to study the joint effects of thermal and mass diffusion behavior on MHD mixed convective flow of a Casson fluid with convective boundary conditions in the boundary layer. Such a study has notable applications in real-world problems to enhance scientific expertise, develop new technologies, strengthen security, safety, and contribute significantly to health. It also has further applications in the fields of transport, biomedical, chemical engineering, paper production, microelectronics, and biomechanics, as well as industrialized methods such as metal spinning, nuclear squandering, polymer extrusion, refining of waste plastic, transpiration cooling process, the oil recovery process, etc.

2. Materials and Methods

2.1. Mathematical formulation.

Consider a Steady two-dimensional MHD mixed convective flow of a Casson fluid with a constant free stream velocity U_∞ and temperature T_∞ over a static permeable flat surface is considered. The x -axis is measured upwards along with the vertical plate, and y -axis is exactly normal(perpendicular) to it as shown in the problem's geometry and u, v be the corresponding velocity components.

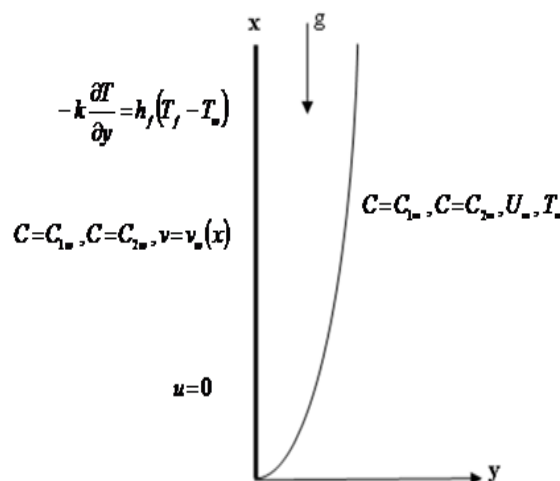


Figure 1. Physical model.

It is assumed that two distinct chemical elements S_m ($m=1, 2$) having a concentration C_m ($m=1, 2$) are dissolved in the solution. Also, the left side of the plate is maintained with a constant fluid temperature T_f , which offers a variable heat transfer h_f . Assisting flow corresponds to the plate being heated by the fluid ($T_f > T_\infty$), and opposing flow corresponds to the plate being cooled by the fluid ($T_f < T_\infty$). The buoyancy approximation is taken into account and is coupled with the flow field. A moving magnetic field $B(x)$ is imposed normally on the surface. The induced magnetic field is not considered due to the very low magnetic Reynolds number when comparing the imposed magnetic field.

Under these assumptions, the basic governing PDE's equations are:

$$\frac{\partial u}{\partial x} + \frac{\partial v}{\partial y} = 0, \quad (1)$$

$$u \frac{\partial u}{\partial x} + v \frac{\partial u}{\partial y} = \nu \left(1 + \frac{1}{\beta} \right) \frac{\partial^2 u}{\partial y^2} - \frac{\sigma}{\rho} [B(x)]^2 u + g \left[\beta_T (T - T_\infty) + \beta_{C_1} (C_1 - C_{1\infty}) + \beta_{C_2} (C_2 - C_{2\infty}) \right], \quad (2)$$

$$u \frac{\partial T}{\partial x} + v \frac{\partial T}{\partial y} = \alpha \frac{\partial^2 T}{\partial y^2}, \quad (3)$$

$$u \frac{\partial C_1}{\partial x} + v \frac{\partial C_1}{\partial y} = D_{S_1} \frac{\partial^2 C_1}{\partial y^2}, \quad (4)$$

$$u \frac{\partial C_2}{\partial x} + v \frac{\partial C_2}{\partial y} = D_{S_2} \frac{\partial^2 C_2}{\partial y^2}, \quad (5)$$

and the appropriate BC's are

$$u = 0, \quad v = V_w(x), \quad C_1 = C_{1w}, \quad C_2 = C_{2w}, \quad -k \frac{\partial T}{\partial y} = h_f (T_f - T_w), \quad \text{at } y = 0, \\ u \rightarrow U_\infty, v \rightarrow 0, \quad C_1 \rightarrow C_{1\infty}, C_2 \rightarrow C_{2\infty}, \quad T \rightarrow T_\infty \quad \text{as } y \rightarrow \infty. \quad (6)$$

Where, $V_w(x) < 0$ and $V_w(x) > 0$ represents suction and injection, respectively.

The rheological equation for an isotropic incompressible Casson fluid [25, 27] is defined as

$$\tau_{ij} = \begin{cases} 2(\mu_B + p_y / \sqrt{2\pi}) e_{ij}, & \pi > \pi_c \\ 2(\mu_B + p_y / \sqrt{2\pi_c}) e_{ij}, & \pi < \pi_c \end{cases} \quad (7)$$

Introducing the following similarity transformation in order to express PDE's (1)-(6) in linear form

$$\psi = (\nu x U_\infty)^{1/2} f(\eta), \quad \eta = y \left(\frac{U_\infty}{\nu x} \right)^{1/2}, \quad \theta(\eta) = \frac{T - T_\infty}{T_f - T_\infty}, \quad \phi_1(\eta) = \frac{C_1 - C_{1\infty}}{C_{1w} - C_{1\infty}}, \quad \phi_2(\eta) = \frac{C_2 - C_{2\infty}}{C_{2w} - C_{2\infty}}, \quad (8)$$

where, ψ is the stream function, and the velocity components are given by

$$u = U_\infty f'(\eta), \quad v = -\frac{1}{2} \sqrt{\frac{U_\infty \nu}{x}} [f - \eta f'] \quad (9)$$

Substituting equations (8) and (9) in Eqn's. (1) - (6) to a set of ordinary differential equations in the non-dimensional form

$$\left(1 + \frac{1}{\beta} \right) f'''' + \frac{1}{2} f f'' - M^2 f' + \lambda [\theta + N_1 \phi_1 + N_2 \phi_2] = 0, \quad (10)$$

$$\theta'' + \frac{\text{Pr}}{2} f \theta' = 0, \quad (11)$$

$$\phi_1'' + \frac{Sc_1}{2} f \phi_1' = 0, \quad (12)$$

$$\phi_2'' + \frac{Sc_2}{2} f \phi_2' = 0. \quad (13)$$

and the distorted boundary conditions are given by

$$f(\eta) = f_w, \quad f'(\eta) = 0, \quad \theta'(\eta) = -a[1 - \theta(\eta)], \quad \phi_1(\eta) = 1, \quad \phi_2(\eta) = 1 \quad \text{at } \eta = 0, \quad (14)$$

$$f'(\eta) = 1, \quad \theta(\eta) = 0, \quad \phi_1(\eta) = 0, \quad \phi_2(\eta) = 0 \quad \text{at } \eta = \eta_\infty,$$

where, η_∞ is the edge of the boundary layer; $M = B_0 \sqrt{\sigma / \rho U_\infty}$ is the magnetic parameter; $\text{Pr} = \nu / \alpha$ is the Prandtl number; $Sc_1 = \nu / D_{s_1}$ and $Sc_2 = \nu / D_{s_2}$ are the Schmidt numbers of the solutals S_m ($m=1,2$) respectively; $\lambda = \lambda(x)$ is the mixed convection parameter and $N_1 = N_1(x)$ and $N_2 = N_2(x)$ are the buoyancy force parameters for concentration C_m ($m=1,2$), which are given by

$$\lambda(x) = \frac{Gr_x}{\text{Re}_x^2}, \quad N_1(x) = \frac{Gr_{x_1}}{\text{Re}_x^2}, \quad N_2(x) = \frac{Gr_{x_2}}{\text{Re}_x^2}. \quad (15)$$

Also, $Gr_x = g\beta_T(T_f - T_\infty)x^3/\nu^2$, $Gr_{x_1} = g\beta_{C_1}(C_{1w} - C_{1\infty})x^3/\nu^2$ and $Gr_{x_2} = g\beta_{C_2}(C_{2w} - C_{2\infty})x^3/\nu^2$ are local Grashof numbers, and $\text{Re}_x = U_\infty x / \nu$ is the local Reynolds number. Mixed convection parameter corresponds to assisting flow, when $\lambda > 0$, and opposing flow when $\lambda < 0$. The skin friction coefficient C_{fx} , the Nusselt number Nu_x , and the Sherwood numbers Sh_{x_1} , Sh_{x_2} are defined as,

$$C_{fx} = 2\text{Re}_x^{-1/2} f''(0), \quad \text{Re}_x^{-1/2} Nu_x = -\theta'(0),$$

$$Sh_{x_1} = -\text{Re}_x^{-1/2} \phi_1'(0), \quad Sh_{x_2} = -\text{Re}_x^{-1/2} \phi_2'(0). \quad (16)$$

3. Results and Discussion

To understand the physics of the model, the flow equations (10) - (13) are solved along (14) using the fourth-order Runge-Kutta integral scheme of shooting technique with the help of the Newton-Raphson method, and results are discussed through plots. This iterative process is repeated by choosing the value of η sufficiently small at each time until the error becomes less than a predefined tolerance up to six decimal places of accuracy. In the present numerical study. The fluid properties such as velocity, temperature, concentration, skin friction as well as heat transfer rate are discussed for various non-dimensional parameters

$$f_w (-0.4 \leq f_w \leq 0.4), \quad \lambda (1 \leq \lambda \leq 20), \quad N_1 (0.1 \leq N_1 \leq 15.69), \quad N_2 (-1.36 \leq N_2 \leq 1.36), \quad \text{Pr} (0.7 \leq \text{Pr} \leq 25),$$

$$M (1 \leq M \leq 5), \quad \beta (1 \leq \beta \leq 5), \quad a (1 \leq a \leq 20), \quad Sc_1 (649.19 \leq Sc_1 \leq 949.19), \quad Sc_2 (1946.19 \leq Sc_2 \leq 4946.19)$$

which are involved in the physical model from figures 2-12. To verify the obtained results are correct or not, a comparative study has been done in Table.1 with the available literature [17] and [18] in the absence of few non-dimensional parameters and found good agreement.

Table 1. Comparison of $-\theta'(0)$ for various values of a when $\text{Pr} = 10$, $f_w = 0$, $M = 0$ and $\lambda = 0$.

a	Aziz[17]	Ishak [18]	Present result
0.8	0.3812	0.381191	0.381201
1	0.4213	0.421344	0.421252

a	Aziz[17]	Ishak [18]	Present result
5	0.6356	0.635583	0.635601
10	0.6787	0.678721	0.678711
20	0.7026	0.702563	0.702601

Table 2. Thermo physical properties of NaCl and Sucrose at 25°C [7].

Components	Morality	Weighs%	$\nu(\times 10^{-6})$	$D_s(\times 10^{-9})$	Sc	ΔC	Nc
NaCl	0.01	0.0584	1.003	1.545	649.19	0.0108	-2.48
	0.05	0.2922	1.007	1.502	670.43	0.03	-6.86
	0.1	0.5844	1.011	1.483	681.72	0.05	-11.43
	0.5	2.922	1.031	1.472	700.4	0.4	-91.51
	1.0	5.844	1.058	1.484	712.93	0.5	-114.3
Sucrose	0.01	0.342	1.014	0.521	1946.25	0.0108	-1.36
	0.05	1.7115	1.043	0.468	2226.4	0.03	-3.77
	0.1	3.423	1.08	0.451	2597.4	0.05	-6.28
	0.5	17.115	1.610	0.442	3635.95	0.4	-50.3
	1.0	34.23	3.535	0.466	7585.83	0.5	-62.87

The effect of the Schmidt number ($Sc_i, i=1,2$) on the concentration distribution ($\phi_i, i=1,2$) are shown in Fig. 2(a) and 2(b). It is perceived that the magnitude of concentration profiles with the escalation of Schmidt numbers ($Sc_i, i=1,2$) for both $\phi_1(\eta)$ (Fig. 2(a)) and $\phi_2(\eta)$ (Fig. 2(b)). The above behavior is observed since enhancing Sc the chemical molecular diffusivity, which ensues in less diffusion due to the mass transfer. The local Schmidt number values refer to the thickness of the large species' diffusion and hence to the rise in the thickness of the concentration boundary layer. It should be noticed that when combined with sucrose, the thickness of the species concentration boundary layer for NaCl is found to be greater since the sizes of the ions (Na^+ and Cl^-) are smaller for the salt softened in water relative to Sucrose molecules dissolved in the water. As a consequence, NaCl diffuses deep into the water in comparison to sucrose.

Figure 3 portrays the effect of suction and injection on concentration profiles ($\phi_1(\eta)$) for $N_1 = 0.1$ and $N_2 = -1.36$. It can be seen that in the instance of injection, ($f_w < 0$) the liquid is passed away from the surface, instigating a decrease in concentration gradient as it stabs to continue the comparable concentration near the surface over a trifling region, and this effect is reversed in the case of suction ($f_w > 0$). It is observed that in an instance of suction ($f_w > 0$), the concentration boundary layer thickness declines, and in the case of injection ($f_w < 0$), concentration boundary layer thickness upturns. In particular, a roughly 43% decrease in boundary layer thickness is seen as suction ($f_w > 0$) increases from $f_w = 0.1$ to $f_w = 0.2$. Whereas, approximately 20% increase in boundary layer thickness is observed as injection ($f_w < 0$) increases from $f_w = -0.1$ to $f_w = -0.2$. Similarly, the velocity profile depicted in Fig. 4 shows that suction ($f_w = 0.3$) decreases the velocity boundary layer thickness while injection ($f_w = -0.3$) does the reverse. For example, from Fig. 4 shows that the velocity boundary layer thickness (η_∞) for $\beta = 5.0$ and $f_w = 0.3$ is 6 whereas, $\eta_\infty \approx 7.5$ for $f_w = -0.3$. In the case of injection fluid, a reduction in the velocity gradient is admitted away from the surface, and this effect is reversed in the case of suction. Injection decreases the sheerness of the wall's velocity profile, but the sheerness increases with suction. Furthermore, in Figure 4 that with the rise in the Casson parameter β , the velocity decreases. As increasing β , the fluid flow becomes more viscous, which resulting in fluid velocity reduction. Even, as β raises, the momentum boundary layer thickness reduces. The outcomes shown in Fig. 4 indicate an

approximately 6.5% decrease in velocity as the Casson parameter upturns from $\beta=1.0$ to $\beta=5.0$ for $f_w = -0.3$.

Effects of Prandtl number (Pr), as well as the mixed convection parameter on the temperature and velocity profiles, are depicted in Fig.5 and Fig.6. Figure 5 that as the Prandtl number and the mixed convection parameter increase, the thermal boundary layer thickness reduces. Quantitatively, for $\lambda=3$ and $Pr = 10$, the thermal boundary layer thickness is approximately 1.6, whereas the thermal boundary layer thickness is approximately 1.25 for $Pr = 21$. The fluid's thermal conductivity decreases with a rise in the value of Prandtl number, and hence thermal boundary layer thickness declines. Also, it can be observed that the effect of the Prandtl number decreases with the increase in the value of the buoyancy parameter. For example, approximately 1% decrease in thermal boundary layer thickness is observed as the Prandtl number increases from $Pr = 21$ to $Pr = 25$ $\lambda=21$, whereas about 7% decrease in the thermal boundary layer is observed $\lambda=3$. Fig.6 shows that the buoyancy effect causes overreach in the velocity contour near the wall for lower fluid of Prandtl number fluid ($Pr = 7.0$), but the overreach is absent for the higher value of the fluid Prandtl number ($Pr=10$). With the mixed convection parameter (λ), the overshoot volume proliferates but decreases as the number of Prandtl number increases due to the stumpy viscosity of the fluid, as the added buoyancy force ($\lambda > 0$) functions as a positive pressure gradient, this increases the velocity inside the boundary layer. The overreach is absent for higher Prandtl number fluids because the added viscous fluid makes it less profound to mixed convection parameter (λ).

The impact of the convective parameter (a) on the temperature contour is displayed in Fig.7. It is noticed that as the convective parameter rises, the plate surface temperature increases. As the convective parameter (a) tends to infinity, the solution is the typical solution for the persistent surface temperature. The outcomes can also be perceived from the BC (i.e., $\theta(0)=1$ as $a \rightarrow \infty$). The effect of buoyancy force parameters N_1 and N_2 on different profiles are presented in Fig.8 to 10. The fraction of buoyancy constraints ($N_i, i=1,2$) is cast-off to characterize buoyancy's simulated strength and solutal convection within the stream areas. It can be seen from Fig.8 that the improvement in the buoyancy parameters causes a decrease in the thickness of the boundary layer. From Fig.9, similar behavior is observed for the thermal boundary layer, and an opposite trend is noticed from Fig.10 as increases buoyancy ratio parameters for concentration boundary layer thickness. The buoyancy parameters' positive and negative signs ($N_i, i=1,2$) indicate that the buoyancy parameter caused by concentration and thermal gradient act in the same and opposite direction.

The effects of magnetic parameter (M) and Casson Parameter (β) on the skin friction coefficient $f''(0)$ with f_w for different values are displayed in Fig.11. It is noticed that the local skin friction decreases as the magnetic parameter (M) increases. Also observed that, for $a=20.0$, $Pr=21$, $N_2 = 2.48$, $Sc_1 = 649.19$, $Sc_2 = 1946.19$, $\lambda=1.0$, $\beta=5.0$, $N_1 = -1.36$ approximately 11% decrease in $f''(0)$ is noticed as M increases from 1 to 2 for $f_w = -0.1$. Suction increases skin friction since the particles are drawn near the wall during suction and injection reduces skin friction since fluid particles are carried away from the wall. Approximately 41% increase in skin friction is noticed for an increase in f_w from -0.1 to 0.1 when $M = 1$ and $\beta = 1$. Also, an increase in the Casson parameter (β) causes a decrease in local skin friction coefficient, an average of 30% decrease in $f''(0)$ is observed as the Casson

parameter (β) increases from 1.0 to 5.0. Variation of heat transfer $\theta'(0)$ with a for different values of Prandtl number (Pr) and f_w is displayed in Fig.12. It can be observed that as the Prandtl number increases, the heat transfer at the wall upturns, thereby decreasing in the boundary layer. Also, an approximately 9% increase in heat transfer at the wall is noticed as Pr increases from $Pr = 7$ to $Pr = 10$ for $f_w = 0.2$ and $a = 1.5$. Further, the increase in the value of the convection parameter a increases the surface temperature. It can be observed that the temperature gradient near the wall increases as increasing the convection parameter. Approximately 18% increase in heat transfer at the wall is noticed as a increases from 1.3 to 1.5 for $f_w = 0$ and $Pr = 10$.

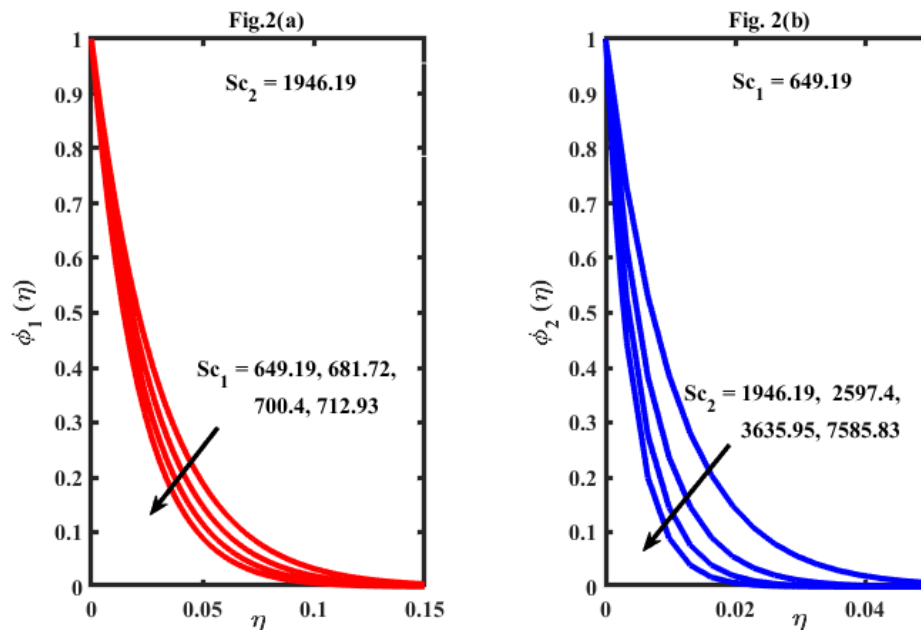


Figure 2. Impact of Sc_1 and Sc_2 on concentration profiles for $M = 0.05, Pr = 7.0, a = 3.0,$
 $\beta = 3.0, N_2 = -1.36, N_1 = 0.1, f_w = 0.1, \lambda = 3.0.$

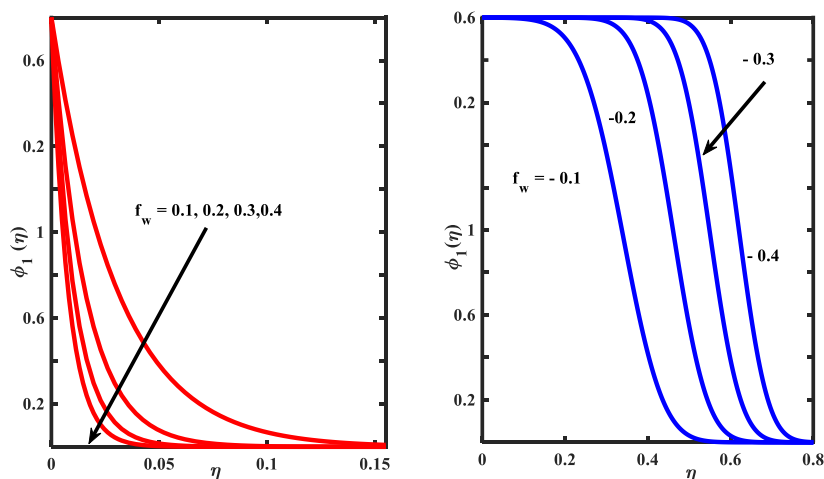


Figure 3. Effect of f_w on concentration profile for $M = 0.05, Pr = 7.0, a = 3.0,$
 $\beta = 3.0, Sc_1 = 649.19, Sc_2 = 1946.19, N_2 = -1.36, N_1 = 0.1, f_w = 0.1, \lambda = 3.0.$

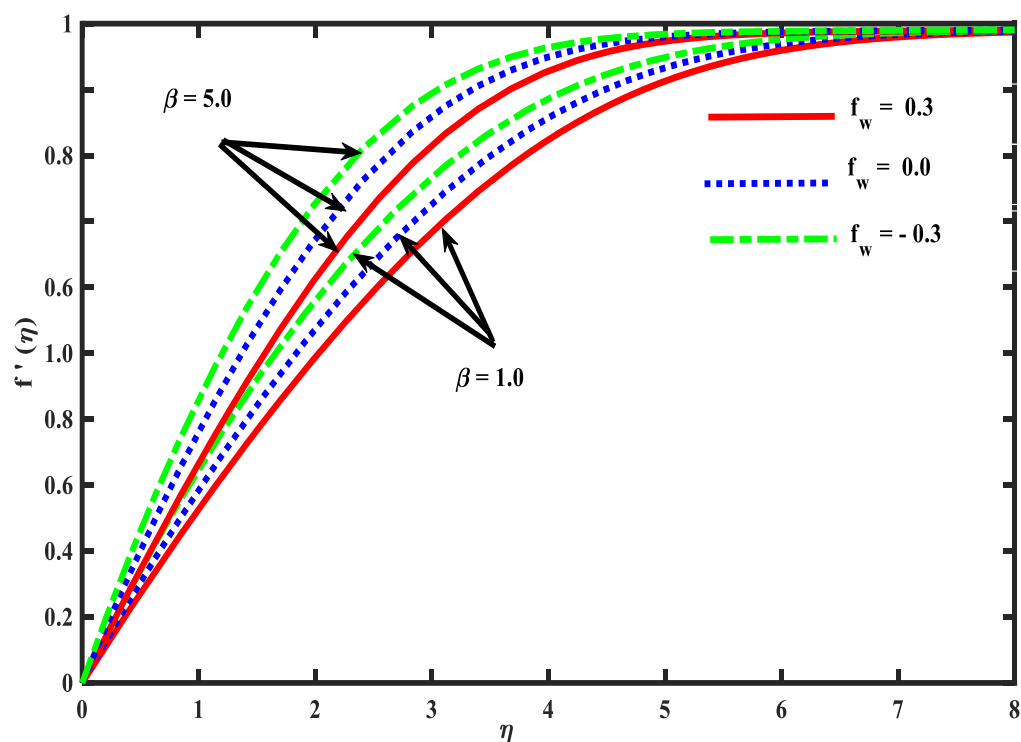


Figure 4. Impact of f_w and β on velocity profile for $M = 0.05, Pr = 0.7, a = 0.5$,
 $Sc_1 = 0.94, Sc_2 = 1.66, N_2 = 0.3, N_1 = 0.1, \lambda = 0.1$.

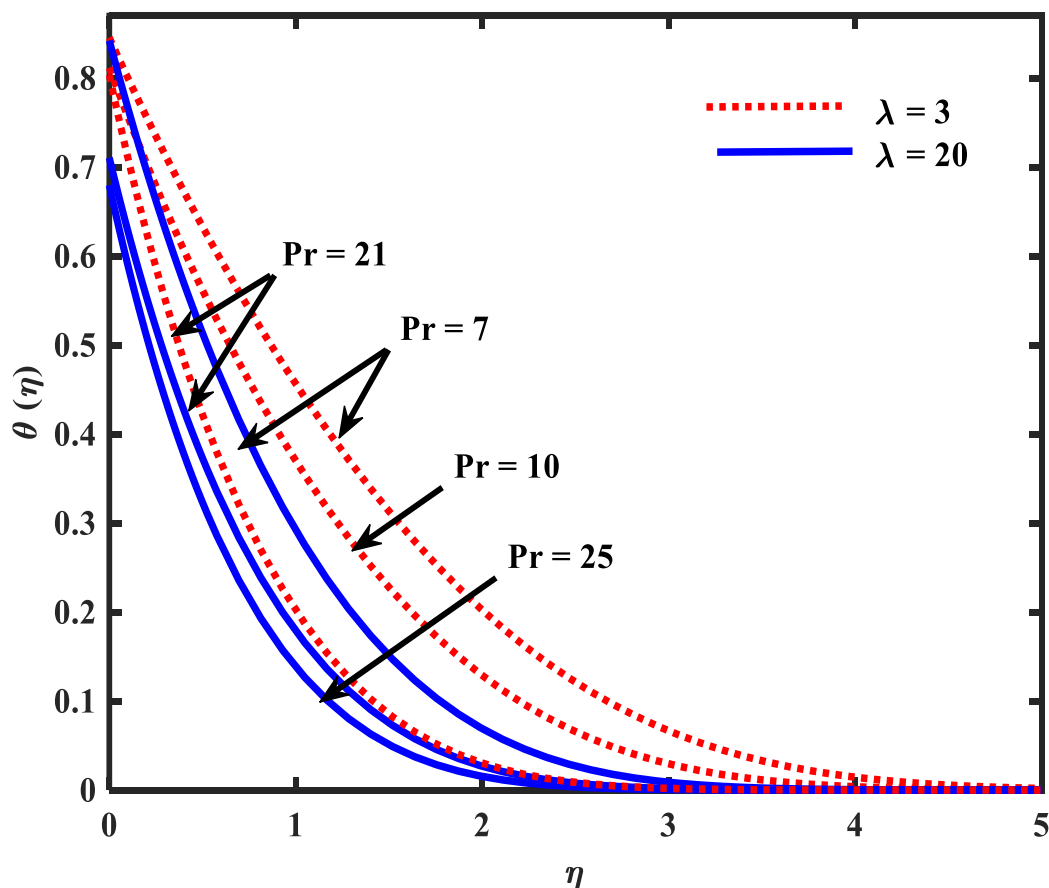


Figure 5. Impact of Pr and λ on temperature profile for $M = 0.05, f_w = 0.1, a = 3.0$,
 $\beta = 3.0, Sc_1 = 649.19, Sc_2 = 1946.19, N_2 = -1.36, N_1 = 0.1$.

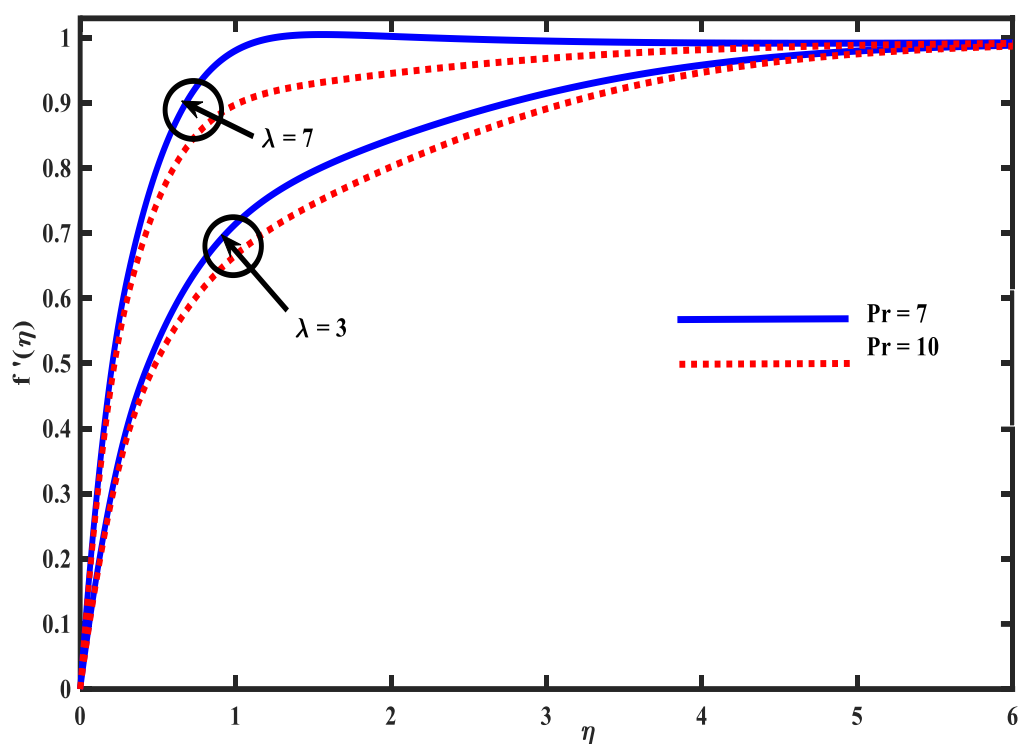


Figure 6. Impact of λ and Pr on velocity profile for $M = 0.05, a = 20.0, Pr = 21, \beta = 3.0, Sc_1 = 649.19, Sc_2 = 1946.19, N_2 = 1.36, N_1 = -0.1, \lambda = 3.0$.

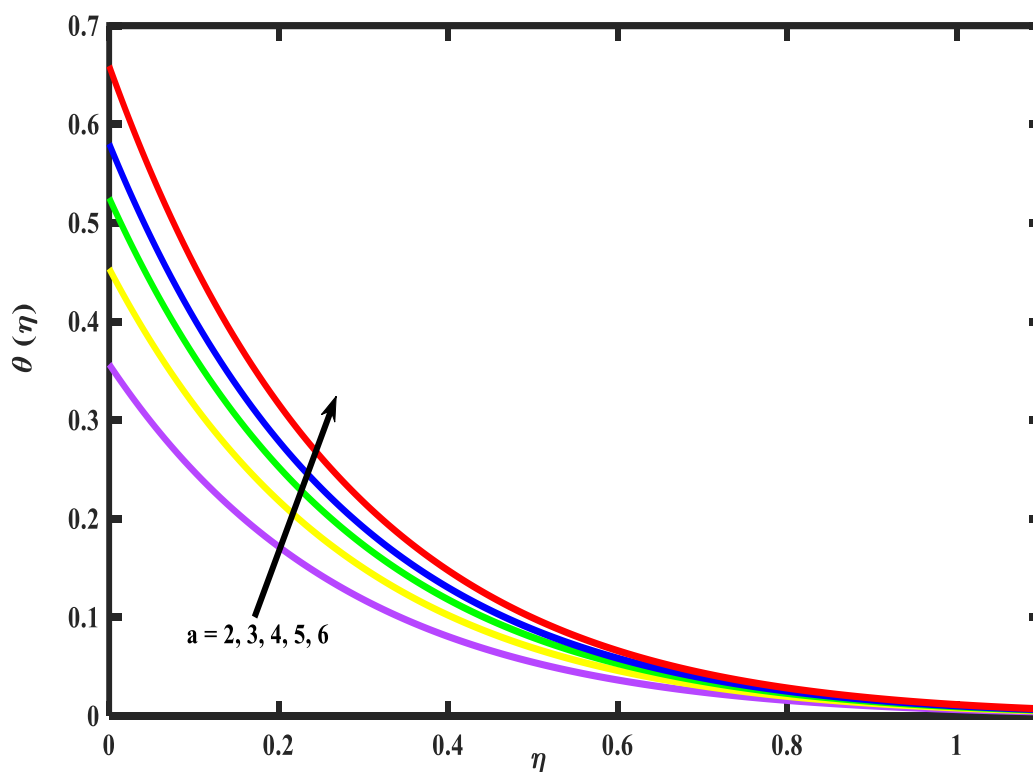


Figure 7. Effect of a on temperature profile for $M = 0.05, Pr = 7, a = 20.0, Sc_1 = 649.19, Sc_2 = 1946.19, N_1 = 0.1, N_2 = -1.36, \lambda = 3.0, f_w = 1$.

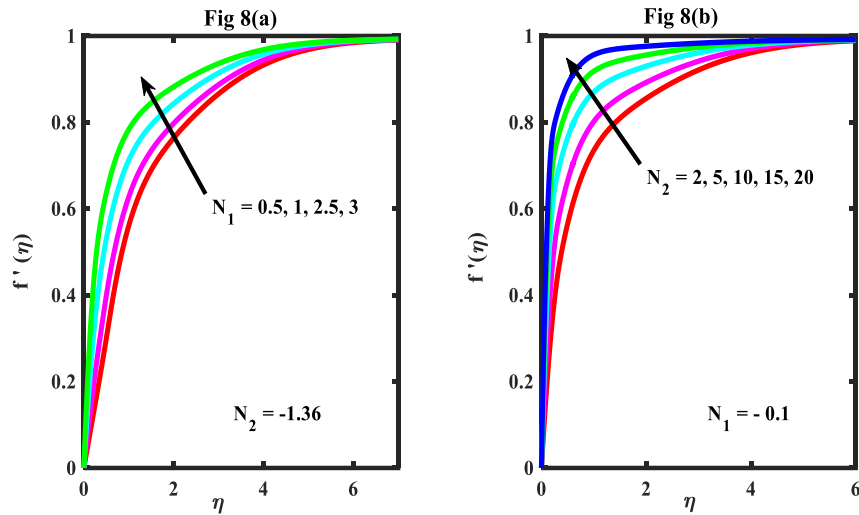


Figure 8. Effect of N_1 and N_2 on velocity profile for $M = 0.05, Pr = 7, a = 20.0$, $Sc_1 = 649.19, Sc_2 = 1946.19, N_1 = 0.1, N_2 = -1.36, \lambda = 3.0, f_w = -0.1, \beta = 1.0$.

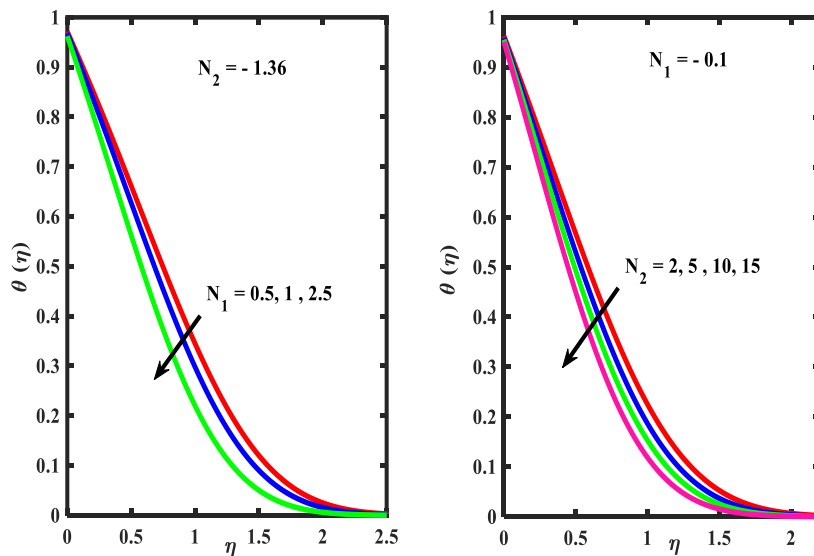


Figure 9. Effect of N_1 and N_2 on temperature profile for $M = 0.05, Pr = 7, a = 20.0$, $Sc_1 = 649.19, Sc_2 = 1946.19, \beta = 1.0, \lambda = 3.0, f_w = -0.1$.

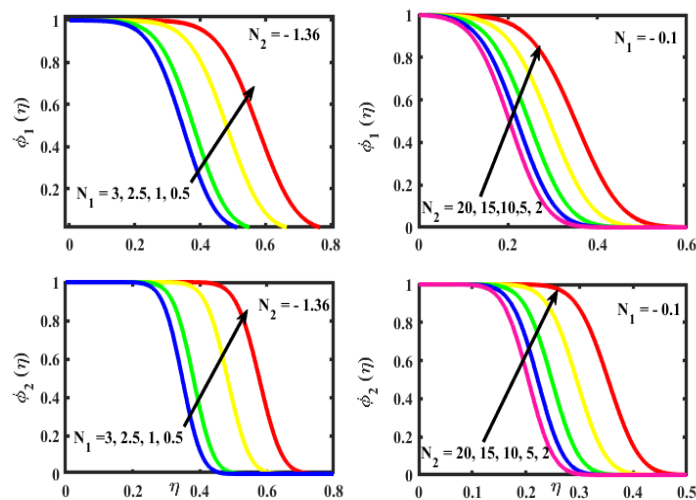


Figure 10. Effect of N_1 and N_2 on concentration profile for $M = 0.05, Pr = 7, a = 20.0$, $Sc_1 = 649.19, Sc_2 = 1946.19, \beta = 1.0, \lambda = 3.0, f_w = -0.1$.

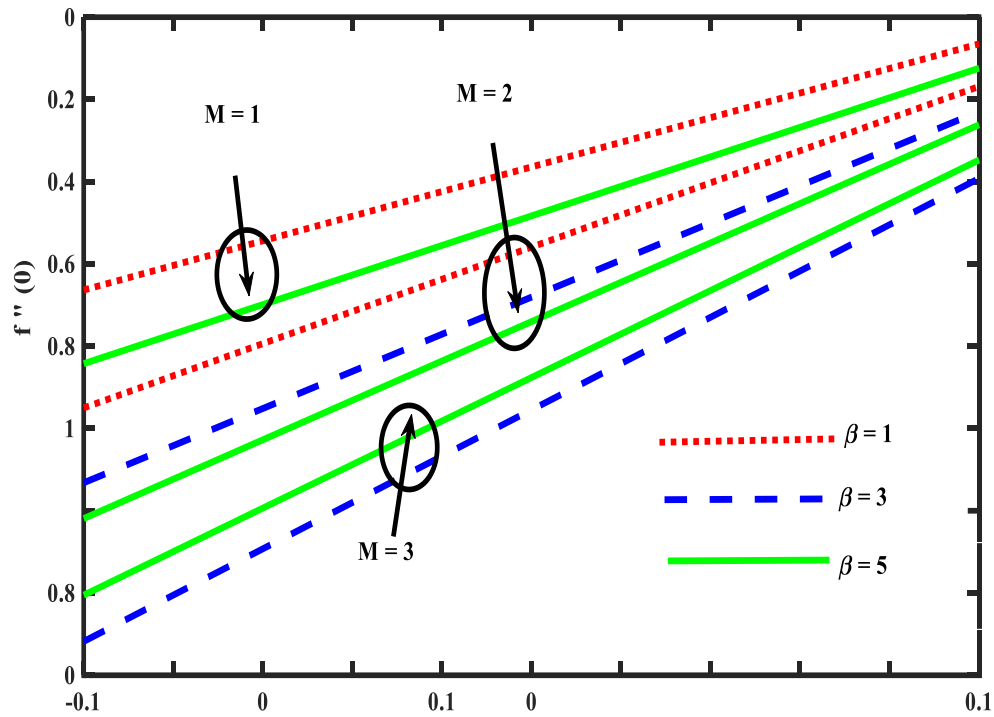


Figure 11. Deviation of $f''(0)$ with f_w for M and β when $Pr = 21, a = 20.0, Sc_1 = 649.19, Sc_2 = 1946.19, \lambda = 1.0, N_1 = -1.36$.

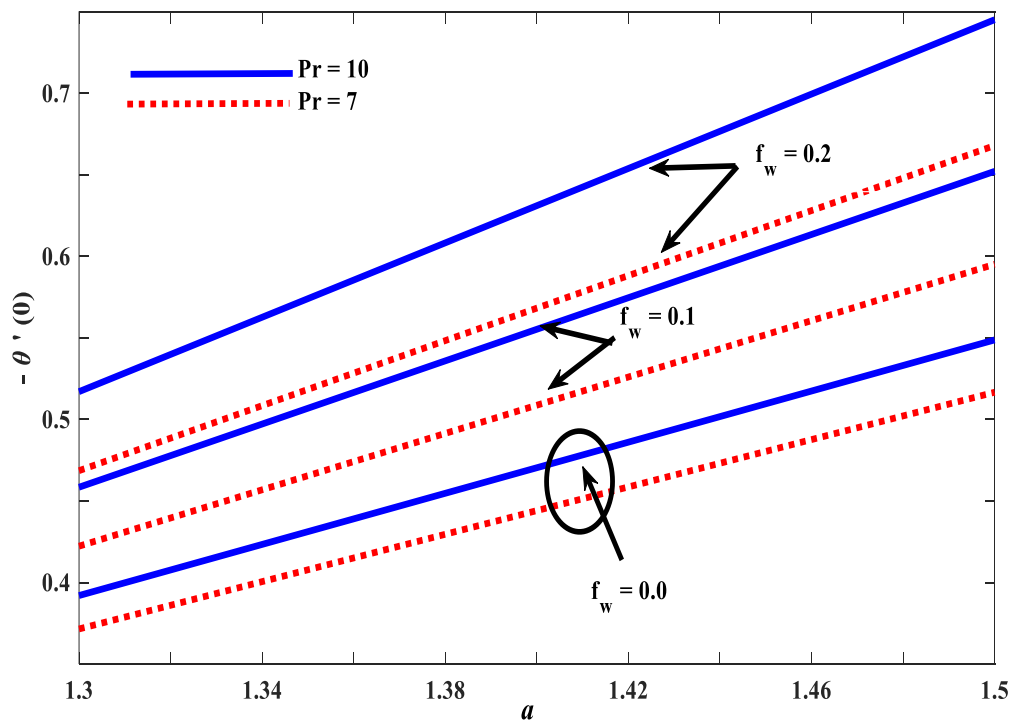


Figure 12. Variation of $-\theta'(0)$ with a for Pr and f_w when $M = 0.05, Sc_1 = 649.19, Sc_2 = 1946.19, \beta = 1.0, \lambda = 3.0, N_1 = 0.1, N_1 = -1.36$.

4. Conclusions

The conclusions of the numerical study are as follows: (i) NaCl concentration boundary layer is thicker than that of sucrose. NaCl diffuses deeper into fluid than sucrose due to the smaller size of ions in NaCl; (ii) Average of 6% decreases in velocity is noticed with the upturn of Casson parameter from $\beta = 1.0$ to $\beta = 5.0$. (iii) Rise in the value of mixed convection parameter (λ) reduces the boundary layer thickness of both velocity, and temperature profile.

Also, the effect λ reduces with the rise in the Prandtl number; (iv) Skin friction at the wall reduces the proliferation in Casson parameter and Magnetic parameter; (v) The convection parameter a increases the surface temperature. An average of 20% growth in heat transfer is noticed at the wall as a it increases from 1.3 to 1.

Funding

This research received no external funding.

Acknowledgments

The authors would like to thank the anonymous reviewers for their valuable comments and suggestions to improve the paper's quality.

Conflicts of Interest

The authors declare no conflict of interest.

References

1. Nield and Bejan, *Convection in porous media*, 4th edition, Springer verlag, **2013**.
2. Kumari, M.; Nath, G. Doubly diffusive unsteady mixed convection flow over a vertical plate embedded in a porous medium. *International Journal of Energy Research* **1989**, *13*, 419-430, <https://doi.org/10.1002/er.4440130406>.
3. Mamou, M.; Bilgen, E.; Gobin, D.; Vasseur, P. Double-diffusive convection in an inclined slot filled with porous medium. *European Journal of Mechanics B, Fluids* **1995**, *14*, 629-652.
4. Patil, P.; Roy, S.; Chamkha, A. Double diffusive mixed convection flow over a moving vertical plate in the presence of internal heat generation and a chemical reaction. *Turkish Journal of Engineering and Environmental Sciences* **2009**, *33*, 193-205, <https://doi.org/10.3906/muh-0905-21>.
5. Murthy, P.V.S.N.; Sutradhar, A.; RamReddy, C. Double-Diffusive Free Convection Flow Past an Inclined Plate Embedded in a Non-Darcy Porous Medium Saturated with a Nanofluid. *Transport in Porous Media* **2013**, *98*, 553-564, <https://doi.org/10.1007/s11242-013-0160-z>.
6. Bandaru, M. Double Diffusive Convection of a Rotating Fluid Over a Vertical Plate Embedded in Darcy-Forchheimer Porous Medium with Non-Uniform Heat Sources. *International Journal of Emerging Trends in Engineering and Development* **2013**, *2*, 415-432.
7. Suresh Babu, R.; Bangalore, R.; P.A, D. Effects of variable fluid properties on a double diffusive mixed convection viscous fluid over a semi infinite vertical surface in a sparsely packed medium. *Frontiers in Heat and Mass Transfer* **2018**, *10*.
8. Rionero, S. Triple diffusive convection in porous media. *Acta Mechanica* **2013**, *224*, 447-458, <https://doi.org/10.1007/s00707-012-0749-2>.
9. Khan, W.A.; Culham, J.R.; Khan, Z.H.; Pop, I. Triple diffusion along a horizontal plate in a porous medium with convective boundary condition. *International Journal of Thermal Sciences* **2014**, *86*, 60-67, <https://doi.org/10.1016/j.ijthermalsci.2014.06.035>.
10. Raghunatha, K.R.; Shivakumara, I.S. Stability of triple diffusive convection in a viscoelastic fluid-saturated porous layer. *Applied Mathematics and Mechanics* **2018**, *39*, 1385-1410, <https://doi.org/10.1007/s10483-018-2376-8>.
11. Patil, P.M.; Shashikant, A.; Momoniat, E.; Harley, C. Numerical simulation of unsteady triple diffusive mixed convection in NaCl-water and Sucrose-water solutions. *International Journal of Heat and Mass Transfer* **2018**, *126*, 147-155, <https://doi.org/10.1016/j.ijheatmasstransfer.2018.05.166>.
12. Patil, P.M.; Roy, M.; Roy, S.; Momoniat, E. Triple diffusive mixed convection along a vertically moving surface. *International Journal of Heat and Mass Transfer* **2018**, *117*, 287-295, <https://doi.org/10.1016/j.ijheatmasstransfer.2017.09.106>.
13. Samuel, N. Triple diffusive flow along a stretching sheet with variable thickness in a porous medium. *Acta Technica CSAV (Ceskoslovensk Akademie Ved)* **2018**, *63*, 407-422.
14. Umavathi, J.C.; Ali, H.M.; Patil, S.L. Triple diffusive mixed convection flow in a duct using convective boundary conditions. *Mathematical Methods in the Applied Sciences* **2020**, *43*, 9223-9244, <https://doi.org/10.1002/mma.6617>.

15. Raghunatha, K.R.; Shivakumara, I.S.; Shankar, B.M. Weakly non-linear stability analysis of triple diffusive convection in a Maxwell fluid saturated porous layer. *Applied Mathematics and Mechanics* **2018**, *39*, 153-168, <https://doi.org/10.1007/s10483-018-2298-6>.
16. Khan, Z.H.; Khan, W.A.; Sheremet, M.A. Enhancement of heat and mass transfer rates through various porous cavities for triple convective-diffusive free convection. *Energy* **2020**, *201*, <https://doi.org/10.1016/j.energy.2020.117702>.
17. Khan, Z.H.; Khan, W.A.; Tang, J.; Sheremet, M.A. Entropy generation analysis of triple diffusive flow past a horizontal plate in porous medium. *Chemical Engineering Science* **2020**, *228*, <https://doi.org/10.1016/j.ces.2020.115980>.
18. Nawaz, M.; Awais, M. Triple diffusion of species in fluid regime using tangent hyperbolic rheology. *Journal of Thermal Analysis and Calorimetry* **2020**, <https://doi.org/10.1007/s10973-020-10026-0>.
19. Mohamed Isa, S.S.P.; Arifin, N.M.; Nazar, R.; Bachok, N.; Ali, F.M. The effect of convective boundary condition on MHD mixed convection boundary layer flow over an exponentially stretching vertical sheet. *Journal of Physics: Conference Series* **2017**, *5*, 949-964, <https://doi.org/10.1088/1742-6596/949/1/012016>.
20. Sharada, K.; Shanker, B. MHD Mixed Convection Flow of a Casson Fluid over an Exponentially Stretching Surface with the Effects of Soret, Dufour, Thermal Radiation and Chemical Reaction. *World Journal of Mechanics* **2015**, *05*, 165-177, <https://doi.org/10.4236/wjm.2015.59017>.
21. Hayat, T.; Shehzad, S.A.; Alsaedi, A.; Alhothuali, M.S. Mixed Convection Stagnation Point Flow of Casson Fluid with Convective Boundary Conditions. *Chinese Physics Letters* **2012**, *29*, <https://doi.org/10.1088/0256-307x/29/11/114704>.
22. John, E.C.; Yakubu, S.I.; Abe-I-Kpeng, G. MHD flow of Casson fluid over a vertical plate embedded in porous media with joule heating and convective boundary condition. *Asian Journal of Mathematics and Computer Resources* **2017**, *19*, 50-64.
23. Raju, R.S.; Reddy, B.M.; Reddy, G.J. Influence of Angle of Inclination on Unsteady MHD Casson Fluid Flow Past a Vertical Surface Filled by Porous Medium in Presence of Constant Heat Flux, Chemical Reaction and Viscous Dissipation. *Journal of Nanofluids* **2017**, *6*, 668-679, <https://doi.org/10.1166/jon.2017.1368>.
24. Muthuraj, R.; Selvi, R.K.; Srinivas, S. Thermodynamic analysis on MHD Casson nanofluid flow in a vertical porous space with stretching walls. *Global Journal of Researches in Engineering* **2018**, *18*, 1-15.
25. Kataria, H.; Patel, H. Heat and mass transfer in magnetohydrodynamic (MHD) Casson fluid flow past over an oscillating vertical plate embedded in porous medium with ramped wall temperature. *Propulsion and Power Research* **2018**, *7*, 257-267, <https://doi.org/10.1016/j.jprr.2018.07.003>.
26. Saqib, M.; Ali, F.; Khan, I.; Sheikh, N.A. Heat and mass transfer phenomena in the flow of Casson fluid over an infinite oscillating plate in the presence of first-order chemical reaction and slip effect. *Neural Computing and Applications* **2018**, *30*, 2159-2172, <https://doi.org/10.1007/s00521-016-2810-x>.
27. Khan, A.; Khan, I.; Khan, A.; Shafie, S. Heat Transfer Analysis in MHD Flow of Casson Fluid Over a Vertical Plate Embedded in a Porous Medium with Arbitrary Wall Shear Stress. *Journal of Porous Media* **2018**, *21*, <https://doi.org/10.1615/JPorMedia.2018018872>.
28. Bhaskar, C.; Sheri, S.; Suram, A. Numerical analysis of MHD casson fluid flow over an exponentially accelerated vertical plate in embedded porous medium with ramped wall temperature and ramped surface concentration in uniform magnetic field. *International Journal of Applied Power Engineering (IJAPE)* **2020**, *9*, 89-99, <http://doi.org/10.11591/ijape.v9.i2.pp89-99>.
29. Sumera, D.; Azizah M.R.; Azizan, S. Triple solutions and stability analysis of mixed convection boundary flow of Casson nanofluid over an exponentially vertical stretching/shrinking sheet. *Journal of Advanced Research in Fluid Mechanics and Thermal Sciences* **2020**, *72*, 94-110, <https://doi.org/10.37934/arfmts.72.1.94110>.
30. Manjappa, A.; Jayanna, G.B.; Chandrappa, P.B. Triple diffusive flow of Casson nanofluid with buoyancy forces and non-linear thermal radiation over a horizontal plate. *Archives of Thermodynamics* **2019**, *40*, 49-69, <https://doi.org/10.24425/ather.2019.12828>.
31. Rao, P.S.; Prakash, O.; Mishra, S.R.; Sharma, R.P. Similarity solution of three-dimensional MHD radiative Casson nanofluid motion over a stretching surface with chemical and diffusion-thermo effects. *Heat Transfer* **2020**, *49*, 1842-1862, <https://doi.org/10.1002/htj.21696>.
32. Lund, L.A.; Omar, Z.; Khan, I.; Raza, J.; Sherif, E.-S.M.; Seikh, A.H. Magnetohydrodynamic (MHD) Flow of Micropolar Fluid with Effects of Viscous Dissipation and Joule Heating Over an Exponential Shrinking Sheet: Triple Solutions and Stability Analysis. *Symmetry* **2020**, *12*, <https://doi.org/10.3390/sym12010142>.
33. Ramanna, S.; Moss, H.G.; McKinnon, E.T.; Yacoub, E.; Helpert, J.A.; Jensen, J.H. Triple diffusion encoding MRI predicts intra-axonal and extra-axonal diffusion tensors in white matter. *Magnetic Resonance in Medicine* **2020**, *83*, 2209-2220, <https://doi.org/10.1002/mrm.28084>.